Regenerative Therapy 26 (2024) 1168–1180

Contents lists available at ScienceDirect

Regenerative Therapy

journal homepage: http://www.elsevier.com/locate/reth

Original Article

Antler blood enhances the ability of stem cell-derived exosomes to promote bone and vascular regeneration

Renjie Zuo [a, 1], Quan Liao [a, 1], Ziwei Ye [b], Chenchun Ding [a], Zhenzhen Guo [b], Junjie He [a], Guoyan Liu [a, b, c, *]

[a] School of Medicine, Xiamen University, Xiamen 361102, Fujian, China
[b] School of Pharmaceutical Sciences, Xiamen University, Xiamen 361102, Fujian, China
[c] Department of Gastrointestinal Surgery, Zhongshan Hospital of Xiamen University, School of Medicine, Xiamen University, Xiamen 361000, Fujian, China

ARTICLE INFO

Article history:
Received 10 June 2024
Received in revised form
22 October 2024
Accepted 8 November 2024

Keywords:
Antler blood
Exosomes
Bone regeneration
Mesenchymal stem cell
Vascular regeneration
miR-21-5p

ABSTRACT

Background: Bone marrow mesenchymal stem cells (BMSC)-derived exosomes (Exos) are important in promoting bone and vascular regeneration. Antler blood (ALB) is a valuable traditional Chinese medicine with potent regenerative effects. However, there is still a lack of clarity regarding the relationship between ALB and BMSC-Exos.

Methods: Primary BMSCs were isolated from SD Rats, and BMSC-derived Exos (BMSC-Exos) were harvested and identified accordingly. ALB was treated with the solution contained pepsin and hydrochloric acid to simulated gastrointestinal digestion *in vitro*. Furthermore, the liquid chromatography-mass spectrometry (LC-MS) was performed to determine the components of digested ALB. Moreover, ALB was utilized to intervene on BMSCs to produce specialized Exos (Exos-ALB), of which the angiogenesis functions were detected both *in vitro* and *in vivo*. For the potential mechanism, both high-throughput sequencing and proteomics were performed.

Results: The main components of ALB consist of amino acids and peptides. Both ALB and BMSC-Exos exhibited significant promotion of bone and blood vessel formation, respectively. Moreover, ALB and BMSC-Exos could increase the expression of BMP-2, RUNX2, and ALP, but reduce the Osteopontin (OPN) expression. Notably, Exos-ALB exhibited the strongest performance in these functions, whereas the presence of miR-21-5p inhibitor can partially counteract the effects of Exos-ALB. The proteomics reveal differential genes associated with bone minimization, angiogenesis, osteoblast differentiation, vesicle-mediated transport, and the Wnt signaling pathway.

Conclusion: ALB enhances the ability of BMSCs-derived Exos to promote bone and vascular regeneration, which may be related to the up-regulation of miR-21-5p.

1. Introduction

The skeletal system is a vital organ in the human body, large defects can limit bone regeneration capacity or result in non-union, leading to substantial negative impacts on the patient's quality of life and psychological well-being [1]. Angiogenesis, a process crucial for bone formation, skeletal development, and osteointegration, plays a significant role in facilitating the transport of growth factors to ensure cell viability and interaction [2]. Among various approaches, the transplantation of bone marrow mesenchymal stem cells (BMSCs) has demonstrated promising outcomes in promoting fracture healing by enhancing both osteogenesis and angiogenesis [3]. Nonetheless, the clinical application of BMSCs still faces challenges due to limitations in cell sources, invasive and painful collection procedures, and safety concerns.

Exosomes (Exos) carry various bioactive molecules such as proteins, nucleic acids, and cytokines, which have specific functions and regulatory effects [4]. Emerging evidence suggests that stem cells derived Exos possess regenerative properties similar to those of stem cells and can be directly used for therapeutic

*Corresponding author. Department of Gastrointestinal Surgery, Zhongshan Hospital of Xiamen University, Xiamen, Fujian, 361000, China.
E-mail addresses: zuorenjie@stu.xmu.edu.cn (R. Zuo), liaoquan@stu.xmu.edu.cn (Q. Liao), yeziwei@stu.xmu.edu.cn (Z. Ye), jsdingdcc@163.com (C. Ding), 32320221154442@stu.xmu.edu.cn (Z. Guo), 24520221154755@stu.xmu.edu.cn (J. He), liuguoyan@xmu.edu.cn (G. Liu).

Peer review under responsibility of the Japanese Society for Regenerative Medicine.

[1] Renjie Zuo and Quan Liao contributed equally to the manuscript and should be considered co-first authors.

https://doi.org/10.1016/j.reth.2024.11.003

purposes, bypassing some of the limitations associated with stem cell transplantation therapy [5]. Previous studies have demonstrated that Exos derived from BMSCs (BMSC-Exos) exhibit therapeutic effects in bone regeneration by delivering their cargo of exosomal molecules, mimicking the therapeutic functions of BMSCs [6,7].

Traditional Chinese medicine (TCM) recognizes the interconnectedness of the body's organs and emphasizes the transmission of physiological signals. This is where extracellular vesicles, such as Exos, play a significant role [8]. They have the capability to transmit information and are not subject to rejection, making them freely ingestible by cells [9]. Thus, Exos play a significant role in elucidating the mechanisms underlying the action of TCM. Moreover, several studies have investigated the impact of TCM components on the function of MSC-derived exosomes (MSC-Exos). For instance, the therapeutic effect of Tanshinone IIA on myocardial ischemia/reperfusion injury has been attributed to its ability to enhance the expression of miR-223-5p in MSC-Exos [10]. Similarly, research has demonstrated that Morinda officinalis F.C. How. can inhibit osteoclast differentiation through rat BMSC-derived exosomes, thereby offering a potential treatment strategy for osteoporosis [11]. Consequently, there is considerable interest in exploring strategies to leverage the therapeutic potential of BMSC-Exos to promote bone repair.

Antler blood (ALB) is the extracted blood obtained from harvested deer antlers, providing a nurturing and conducive environment for antler growth and regeneration [12]. ALB is considered a classic and precious medicinal material in ancient Chinese medicine theory, is documented in numerous ancient texts for its purported effects of strengthening tendons, bones, promoting blood circulation, and nourishing essence [13]. Recent studies have suggested that the regenerative capabilities of deer antlers may be attributed to their peptide content [14]. Additionally, research has demonstrated ALB's potential in accelerating wound healing, aiding in skin repair [15,16], and even treating osteoporosis [17–19], These findings suggest the potential of ALB in promoting bone repair. Therefore, in the field of bone regeneration, we have focused our attention on the effective utilization of deer ALB, attempting to explore its deeper implications.

This study aims to explore the potential of ALB in enhancing the ability of BMSCs Exos to promote bone regeneration. Given ALB's positive effects on osteoblast proliferation and differentiation, as well as the crucial role of BMSCs Exos in bone regeneration, we sought to evaluate the role of ALB-treated BMSCs Exos in promoting both bone and blood vessel formation. To achieve this, we utilized cell culture techniques and *in vivo* models. Moreover, high-throughput sequencing and proteomics were also performed to uncover the molecular mechanisms involved. The findings from this study are expected to shed light on the underlying mechanism through which ALB enhances BMSCs Exos in promoting bone regeneration.

2. Materials and methods

2.1. Experimental animals and cells

Eight to ten-week-old male Sprague-Dawley (SD) rats used in the experiments were purchased and housed at the Xiamen University Animal Experiment Center. Fertilized chicken eggs were incubated using standard incubation equipment (1000000 GC-7411A, Mengda, Shandong, China). All animal experiments were conducted strictly in accordance with the approved animal experimental protocols of the Xiamen University Animal Experiment Center. Animal Experiment Ethics Number: XMULAC20240124.

The human umbilical vein endothelial cell line EA.hy926 was obtained from the National Resource Center, while rat bone marrow mesenchymal stem cells (BMSCS) were isolated and identified in our laboratory.

2.2. Preparing ALB enzymatic digestion solution

5 g of freeze-dried deer ALB powder (Jilin Dong'ao Deer Industry Group Co., Ltd) was dissolved in 20 mL of distilled water. Add a certain amount of solution prepared from 250 U/mL pepsin (1 g/50 g ALB) and 0.1 mol/mL hydrochloric acid solution to the deer ALB solution. Adjust the pH to 1.5 and shake at 37 °C and 200 rpm for 2 h, followed by a water bath for 10 min to deactivate the pepsin. Then, centrifuge at 12000 RPM for 30 min, then add pancreatin (1 g/25 g ALB) to the supernatant and adjust the pH to 7.5. Shake for another 4 h, boil to deactivate, centrifuge, and retain the supernatant. Freeze-dry the supernatant to obtain solid deer ALB enzymatic digestion solution, which was then dissolved in ultrapure water with a concentration of 500 μg/mL.

2.3. Acquisition and characterization of exosome

2.3.1. Isolation and identification of mesenchymal stem cells (MSCs)

Following full-body disinfection and anesthetized, the femur was swiftly extracted under aseptic conditions. Subsequently, a small hole was created at the top of the femur's marrow cavity. The marrow cavity was flushed multiple times from top to bottom with a syringe, and the collected bone marrow cells were placed in the culture dish. After 48 h of cultivation, partial and complete medium changes were performed to retain adherent MSCs.

When the cell confluence reaches 80 %, cells are resuspended in PBS buffer with a concentration of 1×10^7 cells/mL. Incubation with the relative antibody (FITC-CD90 (202503, Biolegend), APC/C7-CD29 (102225, Biolegend) and PE/C7-CD45 (202213, Biolegend)) is carried out in the dark for 20 min. Gate conditions are set for $CD29^+$, $CD90^+$, and $CD45^-$. Cells passing through the gate are collected for further cultivation. The flow cytometry sorting process was conducted using the MoFlo Astrios 1EQS (Beckman, Shanghai, China).

2.4. Extraction and identification of Exos

In this experiment, ultracentrifugation was used for exosome isolation. MSCs were divided into two groups for cultivation: one group served as the control (Exos) with the addition of PBS buffer, while the other group was stimulated with deer ALB enzymatic digest solution at a concentration of 100 μg/mL for 4 days. After intervention, the cell culture supernatants were collected and preserved for exosome extraction. Exos were extracted using differential ultracentrifugation, as described in previous publications [20,21].

According to the guidelines established by the International Society for Extracellular Vesicles (ISEV) in 2014, the identification of Exos relies on three criteria: transmission electron microscopy (TEM), nanoparticle tracking analysis (NTA), and Western blot (WB) analysis targeting the expression of TSG101, CD63, and Calnexin [20,21]. After exosome extraction, the concentration was determined to be 2.5×10^{10} particles/mL. Subsequently, the Exos were diluted to a controlled concentration of 5×10^9 particles/mL for the following experiments.

2.5. CCK-8 assay and PKH67 staining

During the logarithmic growth phase, BMSCS and EA.hy926 cells were seeded onto a 96-well plate to achieve a cell density of

3000 cells/well. Following cell attachment, different pharmacological concentrations of ALB enzymatic digestion solution were added, and the cells were further cultured in the incubator. After 12, 24, and 48 h of drug treatment, the culture medium was replaced with fresh culture medium (100 μL), followed by the addition of 10 μL of CCK-8 reagent. The cell were then incubated for an additional 2 h. Subsequently, the optical density (OD) at 450 nm wavelength of each well was measured using a microplate reader.

The exosome suspension was stained with PKH67 dye and incubated for 30 min to allow dye binding. The exosome suspension was added to the cells for co-culture. Following incubation, cells were collected for fluorescence microscopy observation.

2.6. Bone regeneration experiment

2.6.1. Alizarin red S staining and alkaline phosphatase (ALP) staining

. In this study, MSCs were divided into four groups: the Control group without the addition of ALB enzymatic digestion solution, the ALB group with direct addition of ALB enzymatic digestion solution and osteogenic induction medium (PD-008, Procell, Wuhan, China), the Exos group with addition of Exos derived from normal MSCs and osteogenic induction medium, and the Exos-ALB group with addition of Exos produced by MSCs stimulated by ALB enzymatic digestion solution and osteogenic induction medium. Each group was cultured for 12 days in the incubator to prevent complete differentiation. The induction time for ALP staining experiment was set to 8 days. The staining solutions used were Alizarin Red S working solution (C0138, Beyotime, Shanghai, China) or ALP staining solution (C3206, Beyotime).

2.6.2. Western blot and qRT-PCR

Cells were collected and proteins were extracted, concentrated, and transferred through a sodium dodecyl sulfate-polyvinylidene fluoride membrane. Subsequently, the membranes were incubated with primary antibodies at 4 °C on a shaker overnight. The next day, after completing the rinsing step, the gel was treated with the secondary antibody for 60 min at room temperature. The membrane was then developed and images were captured using the SUPER ECL detection kit. The protein expression was accessed using ImageJ software (Bethesda, MD). The antibodies used in this study were presented in the Supplementary Table 1.

Cell samples were collected and total RNA was extracted. Reverse transcription and PCR processes were performed using the Hifair@ II 1st strand cDNA synthesis kit purchased from Next Sage Biologics with Hieff® qPCR SYBR Green Master Mix (No Rox), and all operations were done according to the steps of the kit instructions and on ice. The reaction system and parameter settings are described in the Supplementary Table 2.

2.6.3. Animal experiments on bone regeneration and hematoxylin and eosin (HE) staining

The 6-8-week-old male SD rats were divided into three groups, each consisting of 3 rats, and acclimated for one week in the animal experiment center. Polyethylene glycol-polypropylene glycol copolymer (F127) was mixed with sterile distilled water and added to a 96-well cell culture plate to form a gel. Subsequently, aliquots of Exos and Exos-ALB suspension were added and allowed to solidify at 37 °C. The rats were anesthetized in a gas anesthesia box, followed by shaving and disinfection. Using a cranial drill, two 5 mm-diameter holes were created, and the prepared cylindrical gel was filled into the cavities to form the blank-Exos group, blank-(Exos-ALB) group, and Exos-(Exos-ALB) group. The skin was sutured, and the rats were allowed to recover from anesthesia. After 48 h, positron emission tomography and X-ray computed tomography (PET-CT) imaging were performed to confirm the modeling effect. After 8 weeks of feeding, the rats were euthanized by intraperitoneal injection of a high-concentration solution of chloral hydrate, and the skull area was removed and fixed. Finally, high-resolution micro-CT imaging was performed on the skull samples, and software was used for data analysis to evaluate the repair of skull defects.

The skull tissue samples, previously scanned by CT, were fixed in 4 % paraformaldehyde solution for 24 h. Subsequently, decalcification and dehydration were performed before the paraffin embedding. The samples were sliced into 4-micron-thick sections. The sections were then dewaxed and rehydrated, followed by the staining with hematoxylin solution (G1121, Solarbio), as well as the eosin solution (G1121, Solarbio). After dehydration, the sections were then mounted with neutral balsam mounting medium and observed using a microscope.

2.7. Vascular regeneration experiment

2.7.1. In vitro angiogenesis assay

The *in vitro* angiogenesis experiment comprises the scratch assay, tube formation assay, and Transwell cell migration assay.

Scratch Assay: EA.hy926 cells were cultured in a 6-well plate until they reached 100 % confluence. A 200 μL pipette tip was used to create a straight scratch on the cell layer surface. The migration and scratch closure were observed and recorded using a microscope at 0 and 12 h post-scratch.

Tube Formation Assay: Pre-cooled Matrigel was added to a 96-well plate, with 50 μL per well, and incubated for 30 min to solidify. EA.hy926 cells in good condition were seeded at a density of 3000 cells per well on the Matrigel-coated 96-well plate. After adding 50 μL of culture medium, the plate was incubated at 37 °C for 8 h. Tube formation was observed under a microscope, and ImageJ software was used to quantitatively analyze the network density, length, and branching of the tubes.

Transwell Migration Assay: A Transwell plate was used for the migration assay, with high-glucose DMEM and the appropriate drugs added to the lower chamber. EA.hy926 cells were suspended in serum-free DMEM and placed in the upper chamber. The plate was incubated at 37 °C for 24 h. The cells on the lower side were fixed in 4 % paraformaldehyde for 30 min, then stained with crystal violet (C0121, Beyotime), and the number of migrated cells was analyzed using ImageJ software.

2.7.2. Chick embryo chorioallantoic membrane(CAM) angiogenesis assay

The procedure for the *in vivo* angiogenesis experiment involves the following steps: Firstly, 12 fertilized chicken eggs are prepared by wiping the eggshells with potassium permanganate solution and incubated for 24 h with the blunt end up. Secondly, the eggs are divided into 4 groups with 3 eggs each, placed in an incubator at approximately 38.0 °C with a humidity of 55%–70 % for 13 days. After the incubation period, the chicken embryos are carefully removed, and a small window is created at the blunt end. PBS buffer is then gently added through the window to moisten the membrane, and the membrane is peeled off using sterilized ophthalmic forceps to expose the CAM. Subsequently, 40 μL of antler enzymatic solution and two types of exosome suspension are added to the filter paper pieces and placed on the avascular areas of the CAM, with a control group using filter paper containing 0.9 % NaCl solution. The window is sealed with transparent tape, and a small ventilation hole is made with a needle before returning the eggs to the incubator for further cultivation. After 48 h of incubation, the chicken embryos are observed on an egg candler for vascular formation around the filter paper pieces. The CAM is then carefully

dissected and placed in a 6 cm cell culture dish for further observation. The area of the formed blood vessels is calculated and analyzed using ImageJ software.

2.8. Treatment with miR-21-5p inhibitor

The miR-21-5p inhibitor (HY-RI00449) and its negative control were sourced from MedChemExpress. For transfection, when the cell confluence reached 80 %, LipoRNAi™ Transfection Reagent (C0535, Beyotime) was employed to facilitate the delivery of the inhibitor into the cells.

2.9. LC-MS analysis of ALB enzymatic digestion solution

50 μL of ALB enzymatic digestion solution was added to a 3 kDa ultrafiltration centrifuge tube and centrifuged at 12,000 g for 30 min at 4 °C. The filtrate was retained. The data analysis software used was Compound Discoverer 3.3. The chromatographic column used was the Waters UPLC BEH Amide column (1.7 μm, 2.1*100 mm). The mobile phase was set as a solution of 25 mol/L ammonium acetate and 25 mol/L ammonia water (solvent A) and pure acetonitrile (solvent B). The gradient elution was performed as follows: 0–0.5 min, 95 % solvent B; 0.5–7 min, 95%–65 % solvent B; 7–8 min, 65%–40 % solvent B; 8–9 min, 40 % solvent B; 9–9.1 min, 40%–95 % solvent B; 9.1–12 min, 95 % solvent B. The flow rate was set at 500 μL·min-1, column temperature at 40 °C, and the injection volume was 3 μL in positive ion scanning mode and 4 μL in negative ion scanning mode. Mass spectrometry conditions: Thermo mass spectrometer was used for primary and secondary mass spectrometry data collection. The mass-to- charge ratio scan range was set to 100–1200, with collision energy at 30 eV. The parameters for the ion source (ESI) were as follows: gas pressure for nebulization (GS1) was set to 60 Psi, auxiliary gas pressure was 60 Psi, curtain gas pressure was 35 Psi, temperature was 650 °C, and spray voltage was 5,000V (in positive ion scanning mode) and −4000V (in negative ion scanning mode).

2.10. Exosome sequencing

Prepare three groups of Exos and Exos-ALB samples, labeled SA1/SA2, SB1/SB2, and SC1/SC2, and submit them to the third-party biological company (Novogene) for high-throughput sequencing. Then, use www.targetscan.orghttp://www.targetscan.orgto perform target screening for the detected miRNAs, and conduct GO and KEGG enrichment analysis through https://david-d.ncifcrf.gov/summary.jsp. Filter out non-significant data and sort the remaining results by COUNT in descending order, selecting the top 10.

2.11. miR-21-5p target gene prediction

To identify the potential target genes of miR-21-5p, we utilized the online tool TargetScan (https://www.targetscan.org/). This database predicts the interactions between microRNAs and their mRNA targets based on seed sequence matching and conservation.

2.12. Proteomics

To assess protein expression differences between samples treated with ALB and untreated controls, Exos were dissolved in 8 M urea, with 100 μL per sample. Proteomics analysis was conducted using the Thermo Orbitrap Fusion Lumos at Xiamen University. After filtering out proteins with missing values, 5825 proteins were detected. Statistical analysis with GraphPad 10.1 revealed 528 differential proteins ($P < 0.05$), with 258 upregulated and 270 downregulated in the ALB group compared to the blank NC group. KEGG and GO analyses were performed on the associated genes of these proteins. A heatmap of the TOP 20 significantly regulated proteins was generated, using Log10 (count) values, and KEGG analysis focused on the TOP 10 pathways.

2.13. Statistical analysis

Experimental data were analyzed and plotted using GraphPad Prism 8.0. Results are expressed as Mean ± SD. Group comparisons were performed using the *t*-test and One Way ANOVA, with significance levels indicated as follows: $*P < 0.05$, $**P < 0.01$, $***P < 0.001$, and $****P < 0.0001$.

3. Results

3.1. Acquisition and characterization of exosome

It was observed microscopically that rat BMSCs exhibited morphological diversity, including fibrous, stellate, flattened, and spindle shaped, and had good adhesion ability (Fig. 1A). Flow cytometry analysis utilizing CD45(−), CD90(+), and CD29(+) markers was employed for cell sorting (Fig. 1B). After ultracentrifugation, the extracted material forms a white precipitate along the wall of the centrifuge tube (Fig. 1F). The particles were approximately 40–120 nm in diameter (Fig. 1C–D), had a density of 2.5×10^{10}/mL, and had a cup-shaped appearance under the electron microscope. The surface protein markers TSG101 and CD63 were expressed, while Calnexin was absent (Fig. 1E). These findings confirm that the extracted material is exosome.

3.2. Ingredient identification of simulated gastrointestinal digestion of deer ALB

ALB is used orally as a pharmaceutical product and is digested and absorbed into the human body to exert its pharmacological effects. Therefore, we performed *in vitro* simulated gastrointestinal digestion of deer ALB for *in vitro* experiments, and performed liquid-quantity-mass spectrometry (LQ-MS) analysis of the product for the preliminary detection of the components contained. A total of 23,359 components were detected using LC-MS/MS technique (Fig. 2A), of which 22 components met our screening criteria. These components were mainly composed of amino acids and peptides (Fig. 2B). It is noteworthy that among the identified components, the concentrations of soy isoflavones and baicalein were relatively high. From the liquid-quality results, it is probable that the main active components of deer ALB are peptides, but it has not yet been determined whether it is a single peptide or a synergistic effect of multiple peptides.

3.3. ALB enzyme digest promotes exosome uptake without cytotoxicity

The CCK-8 assay results demonstrated that the ALB enzyme digest was not cytotoxic to BMSCs and EA.hy926 cells. However, growth inhibition was observed at higher concentrations. Consequently, we selected enzyme digest concentrations of 100 μg/mL for BMSCS and 80 μg/mL for EA.hy926 cells for subsequent experimental studies (Fig. 3A). To determine whether the cells could phagocytose the added Exos, we labeled the Exos with green fluorescence using the PKH67 staining solution. Simultaneously, the cell nuclei were stained with DAPI, resulting in blue fluorescence. The images revealed that the green fluorescence (Exos) was surrounded by the blue fluorescence (nuclei),

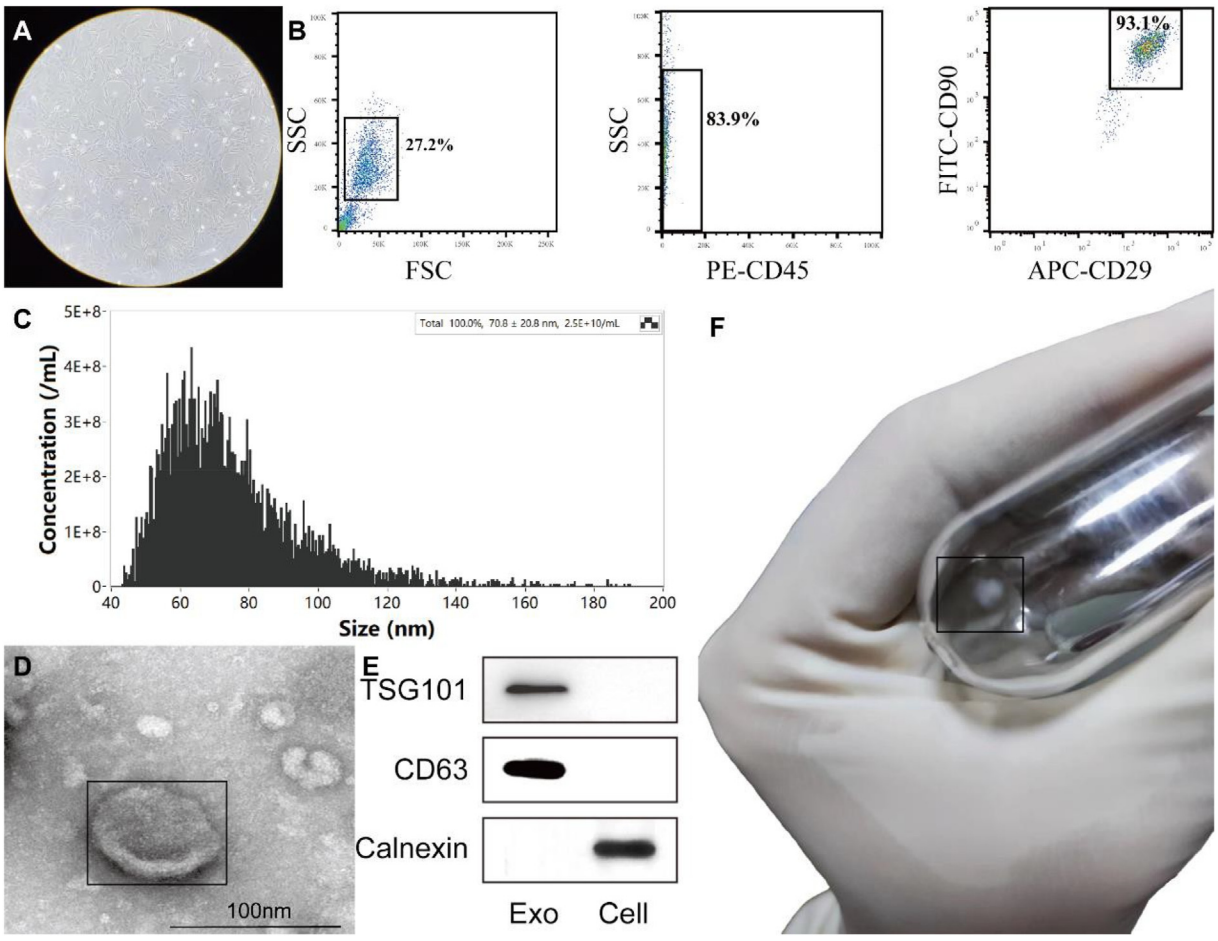

Fig. 1. (A) Microscope was utilized to observe the BMSCS characteristics. (B) Flow cytometric sorting used CD45(−), CD90(+) and CD29(+) as sorting criteria. (C) Nano-flow results to present the extracted precipitate characteristics. (D) Electron microscopy of the precipitate showed a teacup mouth shape morphology. (E) WB results show that the precipitate expresses TSG101 and CD63, but not Calnexin. (F) Cytosolic precipitate attached to the wall of the centrifuge tube.

indicating successful phagocytosis of the Exos into the cytoplasm by the cells (Fig. 3B).

3.4. ALB significantly enhances the function of BMSC-Exos in promoting bone regeneration

Alizarin red staining results indicated that the Exos-ALB group significantly enhanced osteogenesis compared to the Exos group, with the Control group showing the least staining (Fig. 4A). The ALB group was similar to the Exos group, and the ALP staining results were consistent with those of alizarin red staining (Fig. 4A). Western blot and qRT-PCR analysis results indicated that ALP, BMP-2, and Runx2 expression levels in the Exos-ALB group were significantly higher than in the Exos group, indicating a stronger promotion of osteogenic differentiation (Fig. 4B–D). However, Osteopontin (OPN) expression was downregulated, and mRNA detection results were consistent with this finding (Fig. 4B–D).

The cranial defect model results showed that the Exos-ALB group exhibited significantly smaller pore sizes and the fastest bone tissue repair and regeneration; the Exos group did not show a significant bone repair effect (Fig. 4E). HE staining results (Fig. 4F) indicated that the Exos-ALB group had more newly formed mature bone and new blood vessels, the Exos group had continuous bone tissue and new blood vessels, and the Control group had only a small amount of discontinuous bone tissue and fibrous connective tissue.

3.5. ALB significantly enhances the function of BMSC-Exos in promoting angiogenesis

Peripheral vascular regeneration is crucial for bone tissue repair. Results from the scratch assay and Transwell assay showed that both Exos and Exos-ALB enhanced the migration ability of endothelial cells (Fig. 5A and B), with Exos-ALB demonstrating a more significant effect. ALB also exhibited migration-promoting ability, although less prominently. Moreover, VEGF and ANG as key genes related to angiogenesis were selected for the further study. WB results showed that Exos-ALB significantly promoted the expression of VEGF and ANG (Fig. 5C). Further validation through qRT-PCR corroborated these findings (Fig. 5D).

In addition, both tube formation assay (*in vitro*) and the CAM model (*in vivo*) were employed to evaluate peripheral vascular regeneration. Compared to Exos, EA.hy926 cells treated with Exos-ALB showed more pronounced and complete tube formation in the tube formation assay (Fig. 5E). These data suggest that Exos produced under stimulation by ALB enzyme digest have stronger angiogenic potential than normal Exos. Furthermore, results from the CAM model demonstrated that Exos-ALB significantly promoted branching of blood vessels around the filter paper (Fig. 5F). It is noteworthy that direct application of ALB enzyme digest also promoted blood vessel formation, although its ability to promote vessel formation was weaker compared to the exosome group.

A

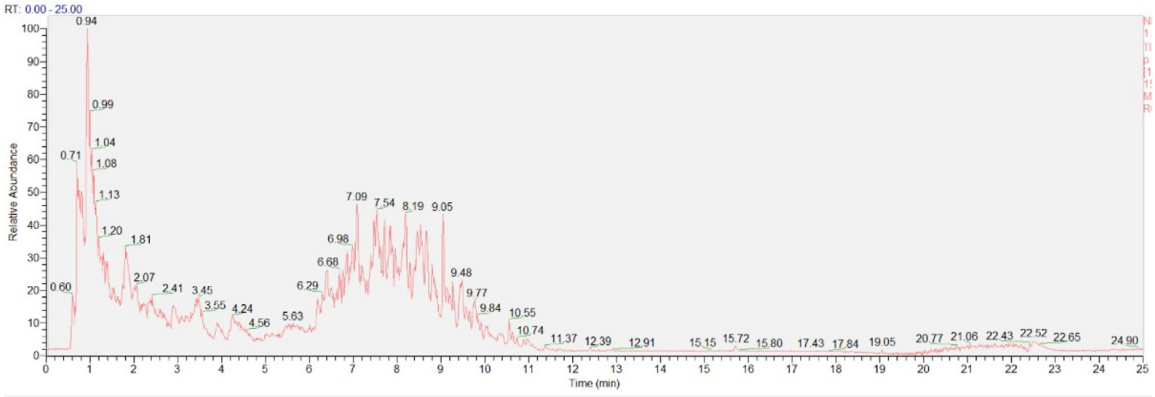

B

	RT [min]	Molecular Weight	Formula	Compound	Area(Max)	mzVault Best Match
1	0.711	174.11168	$C_6H_{14}N_4O_2$	Arginine	732788434.2	93.6
2	0.818	174.11168	$C_6H_{14}N_4O_2$	L-Arginine	545037050.6	97.1
3	0.853	117.07898	$C_5H_{11}NO_2$	L-Valine	92755202.18	91
4	0.932	149.05105	$C_5H_{11}NO_2S$	L-Methionine	76985526.96	93.8
5	1.106	131.09463	$C_6H_{13}NO_2$	Norleucine	587974989.4	95.8
6	1.169	151.04941	$C_5H_5N_5O$	Guanine	94473282.13	94.4
7	1.279	238.09536	$C_{11}H_{14}N_2O_4$	Gly-Tyr	253844392.8	93.9
8	1.282	181.07389	$C_9H_{11}NO_3$	Tyrosine	193733150.2	97.5
9	1.828	165.07898	$C_9H_{11}NO_2$	L-Phenylalanine	5309922471	96.6
10	2.245	202.13174	$C_9H_{18}N_2O_3$	Ala-Ile	3796534946	91.3
11	2.32	188.11609	$C_8H_{16}N_2O_3$	Gly-Leu	803719027.3	91.6
12	3.232	131.09463	$C_6H_{13}NO_2$	Isoleucine	43268457.09	96.4
13	3.55	236.11609	$C_{12}H_{16}N_2O_3$	Ala-Phe	4376166808	94.8
14	8.721	210.13683	$C_{11}H_{18}N_2O_2$	Cyclo(Leu-Pro)	152933153	93.4
15	9.195	433.11347	$C_{21}H_{21}O_{10}$	Pelargonidin-3-O-glucoside	651042146.7	92.6
16	9.286	131.09463	$C_6H_{13}NO_2$	Leucine	20595388.11	98.4
17	10.555	165.07898	$C_9H_{11}NO_2$	Phenylalanine	17344054.81	97.1
18	10.606	254.05791	$C_{15}H_{10}O_4$	Daidzein	172305293.7	96.5
19	10.89	284.06847	$C_{16}H_{12}O_5$	Wogonin	17681283.66	100
20	10.954	372.15863	$C_{22}H_{20}N_4O_2$	3,6-Bis(1H-indol-3-ylmethyl)-2,5-piperazinedione	27160240.04	91.9
21	11.147	333.14773	$C_{20}H_{19}N_3O_2$	3-benzyl-6-(1H-indol-3-ylmethyl)piperazine-2,5-dione	6842981.193	92.6
22	13.264	191.13101	$C_{12}H_{17}NO$	DEET	12722919.56	93.4

Fig. 2. (A) Preliminary determination of the components of ALB enzyme digest by liquid-mass spectrometry. (B) Component selection criteria are: spectrum area is greater than 10,000,000 and mzVault score greater than 90.

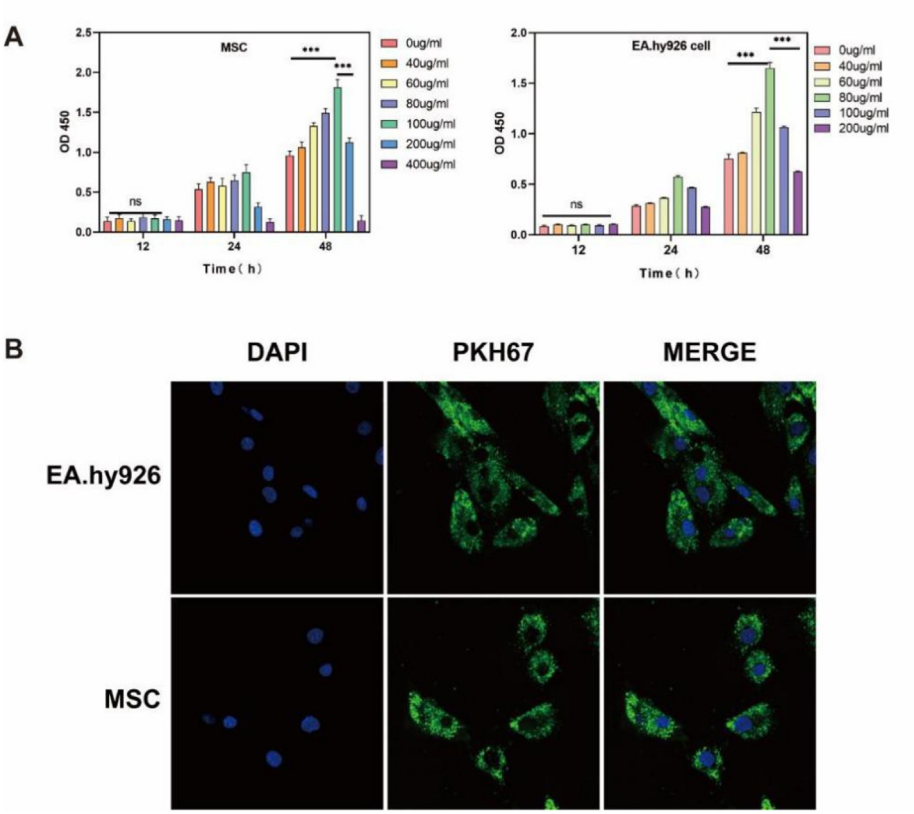

Fig. 3. (**A**) The effect of different concentrations of ALB enzymatic solution on BMSCS and EA.hy926 cell proliferation capacity. NS, not statistically significant. (**B**) Tracking of extracellular vesicles via PKH67 staining. ***$p < 0.001$; Mean ± SEM.

3.6. RNA sequencing reveals miR-21-5p may be involved in the undergoing mechanism of ALB promoting bone regeneration

The above experiments collectively validated that MSCs, upon stimulation with deer ALB enzymatic hydrolysate, produce Exos with significantly enhanced regenerative potential for both bone and vascular tissues. Subsequently, RNA sequencing and comparative analysis were conducted on exosome samples from both groups (Fig. 6A). The sequencing results revealed that the majority of miRNAs did not exhibit significant differences between the two groups of Exos. However, compared to the Exos from the normal group, miR-21-5p was upregulated in Exos generated after deer ALB stimulation (Fig. 6B).

Previous studies have demonstrated the promotive roles of miR-21-5p in both bone [22] and vascular [23] regeneration. Through bioinformatics analysis, we identified 234 potential target genes that miR-21-5p may bind to (Supplementary Table 3). To further explore these targets, we performed Gene Ontology (GO) enrichment analysis, aiming to understand the involved biological processes (BP), molecular functions (MF), and cellular components (CC). We identified a total of 27 enriched MFs, 109 enriched BPs, and 17 enriched CCs (Fig. 6C, $p < 0.05$). The top 10 significantly enriched MFs, BPs, and CCs from the GO analysis are presented in Fig. 6D. Additionally, KEGG pathway enrichment analysis revealed the enrichment of these targets in 22 pathways, with the top 10 enriched KEGG pathways shown in Fig. 6E ($p < 0.05$).

3.7. miR-21-5p inhibitor reduced the expression of both angiogenesis and osteogenesis-related proteins

The miR-21-5p inhibitor was utilized to target and suppress miR-21-5p, and its effects on the expression of angiogenesis- and osteogenesis-related proteins were assessed. As anticipated, the miR-21-5p inhibitor led to a downregulation of angiogenesis-related proteins, such as VEGF and ANG (Fig. 7A), as well as osteogenesis-related proteins, including ALP, RUNX2, and BMP-2 (Fig. 7B). Furthermore, the inhibitor was also able to partially reverse the upregulation of these proteins induced by ALB (Fig. 7A–B).

3.8. miR-21-5p inhibitor reduced the expression of both angiogenesis and osteogenesis-related proteins

Proteomics was employed to identify genes with altered expression following ALB treatment (Fig. 8A). The heat map, which contrasts the NC group with the ALB group, shows clear differences in protein expression between two groups. Proteins such as PCHP_MOUSE (Phosphorylcholine phosphatase) and ALN_MOUSE (Alanyl-tRNA synthetase) exhibit significant upregulation in the ALB group, whereas proteins like LIP_MOUSE (Triacylglycerol lipase) and WRT_MOUSE (Protein Wnt) show downregulation. Pathway enrichment analysis of these differentially expressed genes (Fig. 8B) revealed that the Biological Process pathways were significantly associated with bone minimization, angiogenesis, osteoblast differentiation, vesicle-mediated transport, and the Wnt signaling pathway.

4. Discussion

In this study, ALB was found to demonstrate a capacity to enhance both osteogenesis and angiogenesis *in vitro*. Furthermore, through additional *in vitro* and *in vivo* experiments, we observed that ALB exerted a significant promotion effect on the function of BMSC-Exos in promoting osteogenesis and angiogenesis. To

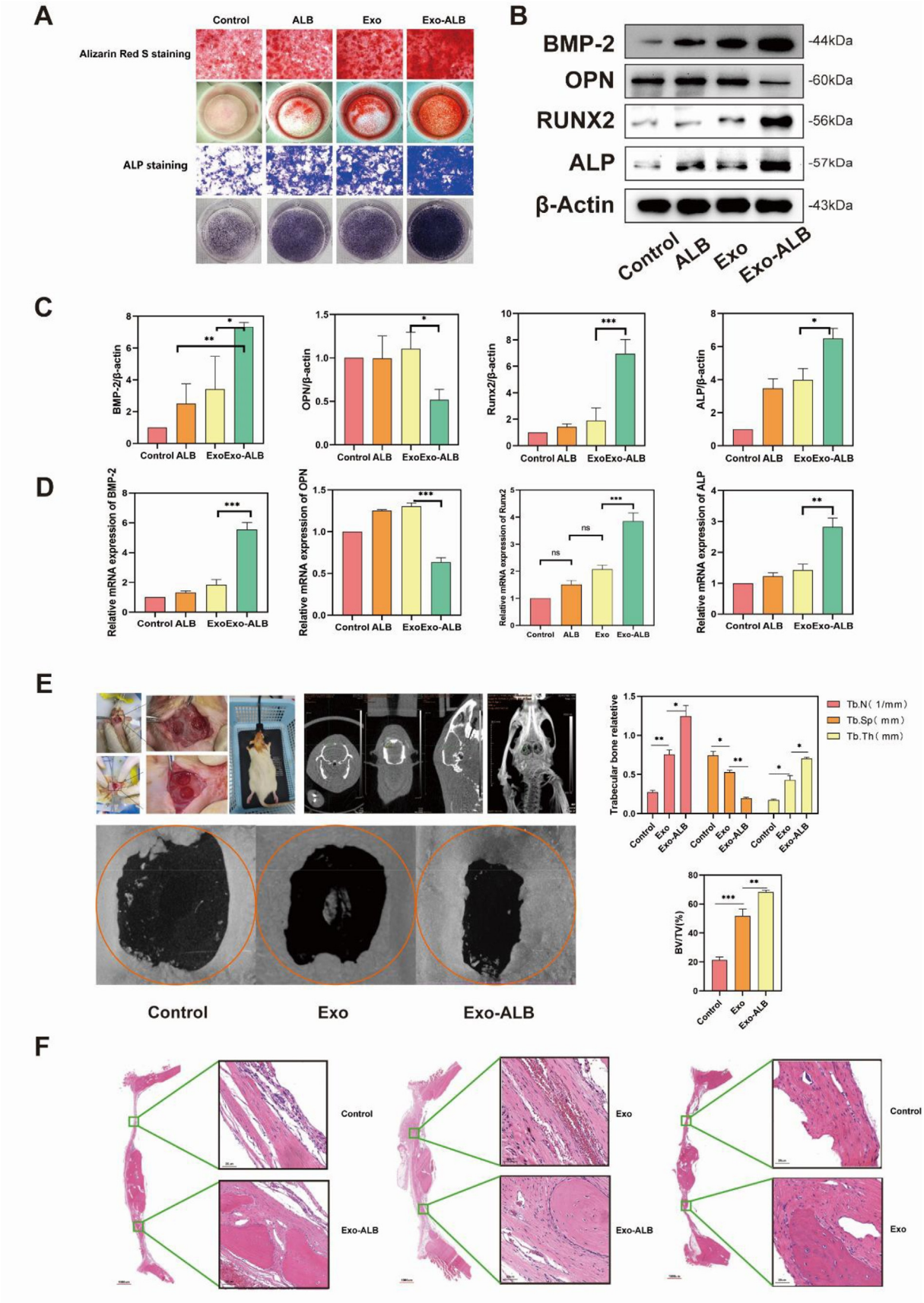

Fig. 4. (**A**) Alizarin Red S staining and ALP staining results. (**B**) Western blot analysis detected the expression levels of osteogenesis-related proteins. (**C**) Analysis of grayscale values of bands corresponding to osteogenesis-related proteins. (**D**) qRT-PCR detected the mRNA expression levels of osteogenic-related genes. (**E**) Establishment of a rat cranial defect model and analysis of experimental results. (**F**) Histological results of HE staining. *, $p < 0.05$; **, $p < 0.01$; ***, $p < 0.001$; Mean ± SEM.

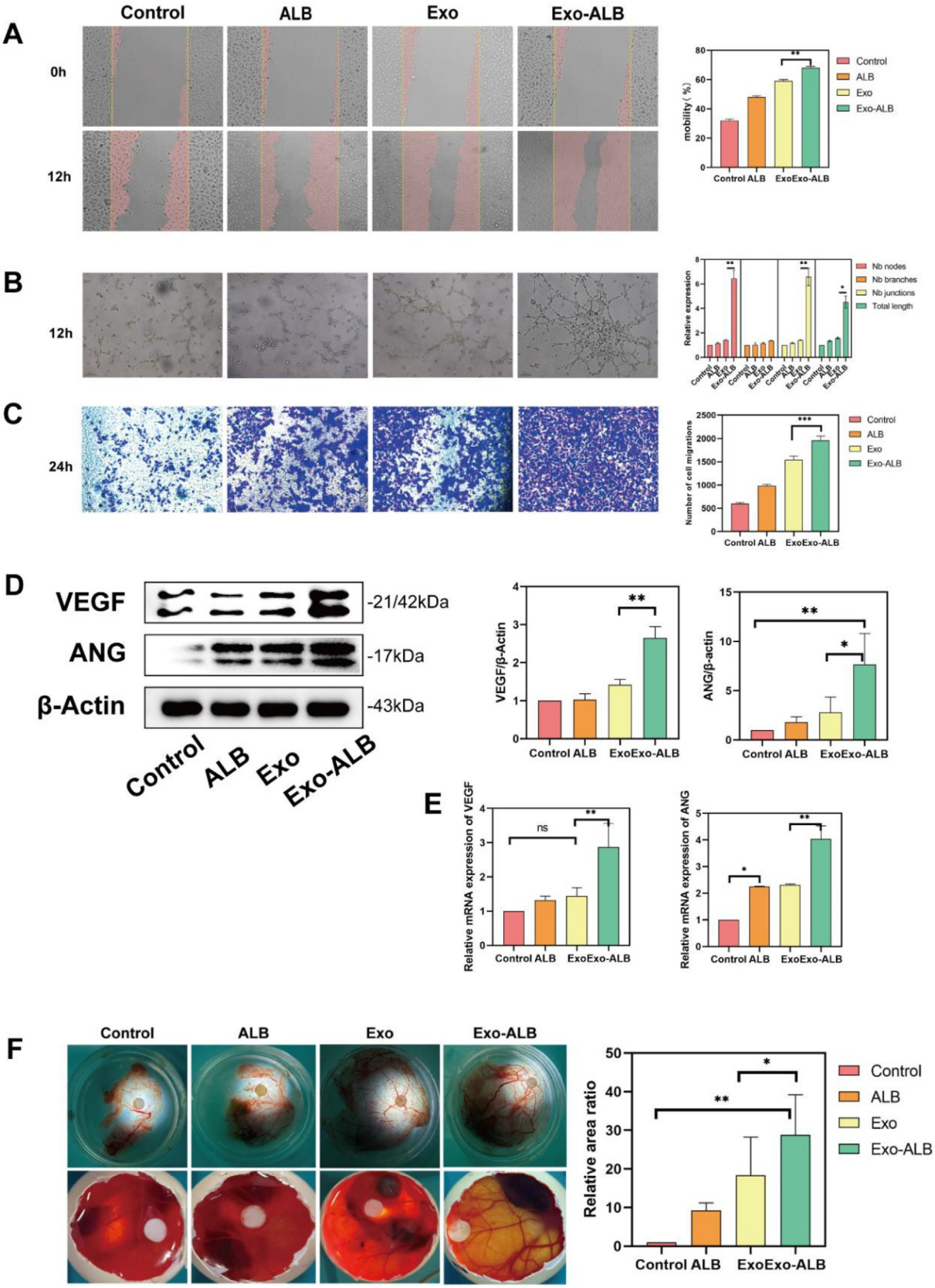

Fig. 5. (**A**) Cell scratch assay and quantitative results. (**B**) Microscopic results of the angiogenesis assay, quantitatively analyzed for vessel formation nodes, branches, and intersection connections. (**C**) Transwell assay, quantitatively analyzed based on the number of migrated cells. (**D**) Western blot detected the expression levels of angiogenesis-related proteins and analyzed band grayscale values. (**E**) qRT-PCR detected the mRNA expression levels of angiogenesis-related genes. (**F**) CAM experiment results and quantification analysis of vascular area. *, $p < 0.05$; **, $p < 0.01$, ***, $p < 0.001$; Mean ± SEM.

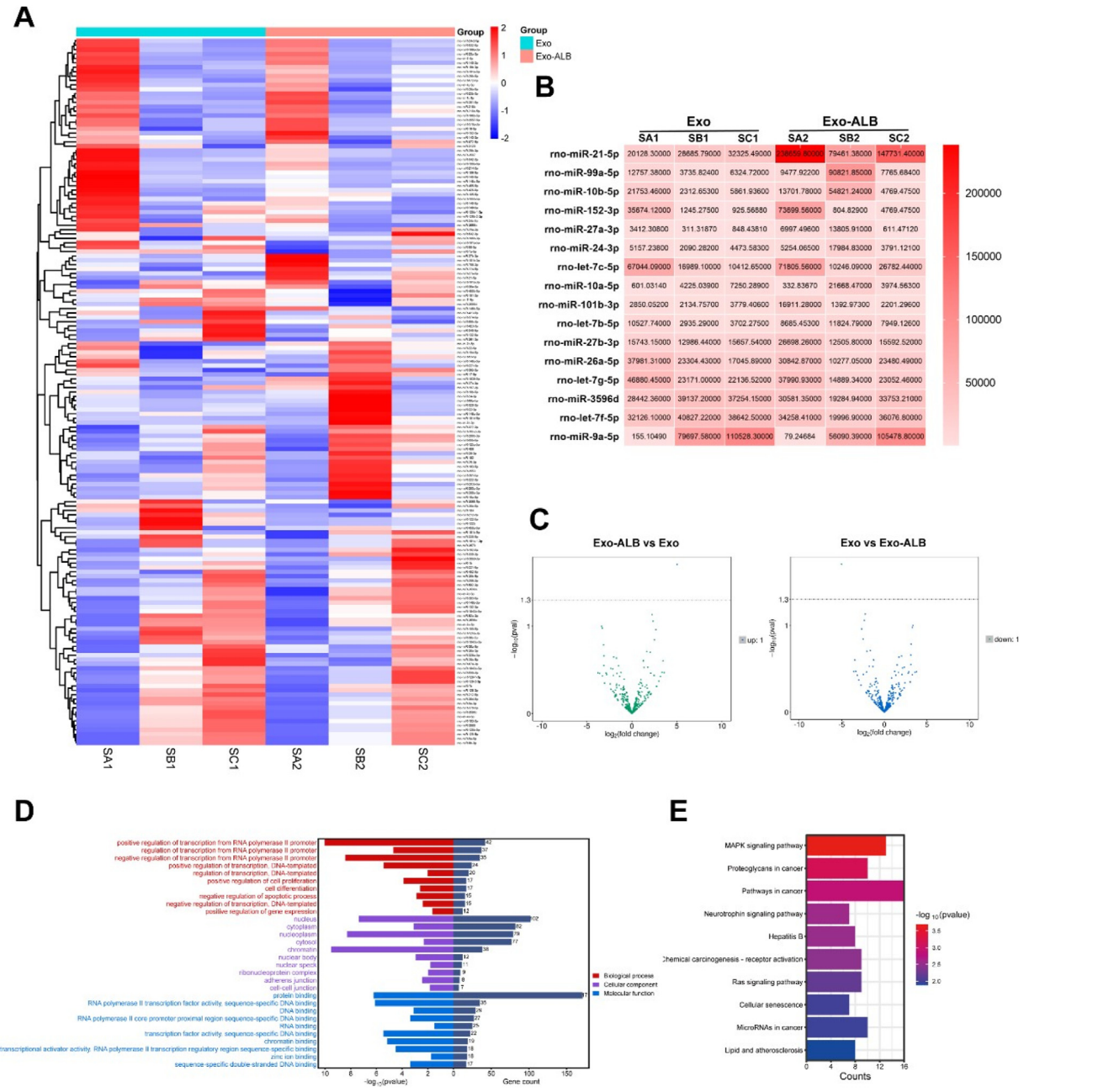

Fig. 6. (**A**) The heatmap displays the results of RNA sequencing. (**B**) The heatmap displays miRNA expression levels (TPM processed). (**C**) Volcano plots depict the distribution of differential miRNA. (**D**) Top 10 terms with significant enrichment in MF, BP and CC. (**E**) Top 10 terms with significant enrichment in KEGG pathway.

investigate the underlying mechanisms, RNA sequencing was employed, revealing that ALB may exert its effects by upregulating miR-21-5p. Additionally, proteomics analysis revealed that differentially expressed genes are closely related to various biological processes, including vesicle-mediated transport and the Wnt signaling pathway.

Adequate blood supply is essential for rapid repair and regeneration of bone tissue [24,25]. Therefore, we conducted research on the vascular formation effects of deer ALB. ALB, found within deer antlers, has an extremely complex composition [26]. Contemporary scientific research focuses on exploring the regenerative functions of deer antlers, with the peptide components believed to be the reason behind their powerful regenerative capabilities [13,27,28]. In this study, we utilized LC-MS to determine its components. After enzymatic digestion, we found that the majority of components were amino acids and peptides, which aligns with previous findings.

In addition to the examination of vascular formation effects, we also investigated the expression levels of other proteins associated with bone growth. One such protein is bone morphogenetic protein 2 (BMP2), which was initially identified in bone and plays a pivotal role in regulating osteoblast differentiation, bone development, and bone repair [29]. Transgenic mice that exhibit overexpression of noggin, an antagonist of BMP2, specifically in osteoblasts, display reduced trabecular bone volume and decreased rates of bone formation [30]. Another important protein we examined is Runx2, which serves as a crucial transcriptional effector during the differentiation, maturation, and normal functioning of osteoblasts,

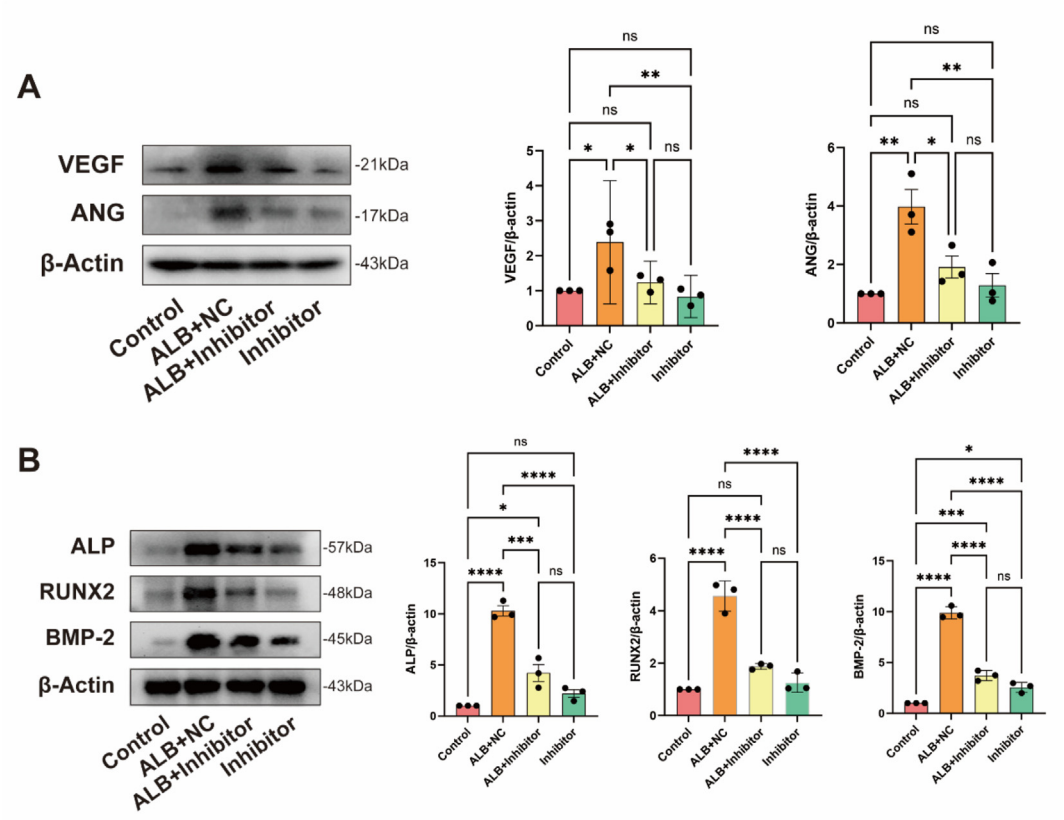

Fig. 7. Western blot was to detect the expression of (**A**) angiogenesis-related and (**B**) osteogenesis-related proteins.

chondrocytes, and mesenchymal stem cells [31]. The mutual induction of Runx2 with the Wnt and Sp7 pathways promotes the differentiation of pre-osteoblasts into immature osteoblasts. Ultimately, Runx2 facilitates the production of bone matrix proteins in immature osteoblasts, leading to complete osteoblast maturation [32]. Furthermore, ALP activity is often considered an indicator of osteoblast presence and new bone formation [33]. In our study, we observed that Exos-ALB significantly upregulated the expression of the aforementioned proteins, suggesting a potential regulatory role of ALB in bone growth processes.

Meanwhile, combining existing data analysis revealed that OPN is unique, it has dual regulatory effects, promoting bone formation while inhibiting bone formation, and participating in key processes such as the migration, adhesion, and degradation of bone matrix by osteoblasts [34]. Recent studies have found a close relationship between OPN and osteoclast (OC) activity [35,36]. The upregulation of osteoclast activity would be detrimental to the repair and regeneration of bone tissue [37]. When OPN expression is upregulated, OC activity is activated and bone formation is inhibited, leading to a decrease in bone mass. The role of OPN in osteogenic differentiation is not fully understood. Based on the experimental results of this study, Exos-ALB significantly downregulated the expression level of OPN, suggesting its correlation with the inhibition of osteoclast activity.

Recent studies on extracellular vesicles have revealed the significant regulatory role of miRNAs in life activities [38]. Therefore, we extracted and collected extracellular vesicles derived from two groups of BMSCS for RNA sequencing studies. The results showed that miR-21-5p was significantly upregulated under the stimulation of deer ALB. Moreover, miR-21-5p could significantly reverse the impact of ALB in promoting both angiogenesis and osteogenesis-related proteins. Related research indicates that miR-21-5p may play an important role in promoting bone and vascular regeneration [39,40]. Thus, we propose that miR-21-5p may be an important mediator for deer ALB to exert its function in promoting bone and vascular regeneration.

The proteomics results revealed that differentially expressed genes were associated with several biological processes, including the Wnt signaling pathway. Prior research has established a connection between miR-21-5p and the Wnt signaling pathway [41,42]. For instance, in fluoride-induced osteoblast activation, miR-21-5p activates the canonical Wnt signaling pathway by targeting PTEN and DKK2 [41]. Additionally, genes differentially expressed following ALB treatment were linked to bone minimization, angiogenesis, osteoblast differentiation, and vesicle-mediated transport. These findings reinforce the association of ALB with bone repair and Exos. Future research will focus on further elucidating the underlying molecular mecanisms.

The significance of this study lies in its pioneering exploration of the impact of ALB on stem cell Exos. By examining the effects of ALB on stem cell Exos, we aim to contribute to the current understanding of the regenerative potential of ALB and its underlying mechanisms. However, it is important to acknowledge the limitations of our study. Although we have provided preliminary insights into the potential mechanism involved, further investigations are necessary to fully elucidate the intricate workings and pathways underlying the observed effects. For example, additional analysis is needed to identify the specific active amino acids or peptides responsible for the regenerative effects of ALB, as well as to establish the relationship between OPN and OC. Additionally, further research is needed to clarify whether ALB acts directly on angiogenesis to promote bone regeneration or if it promotes BMSC-

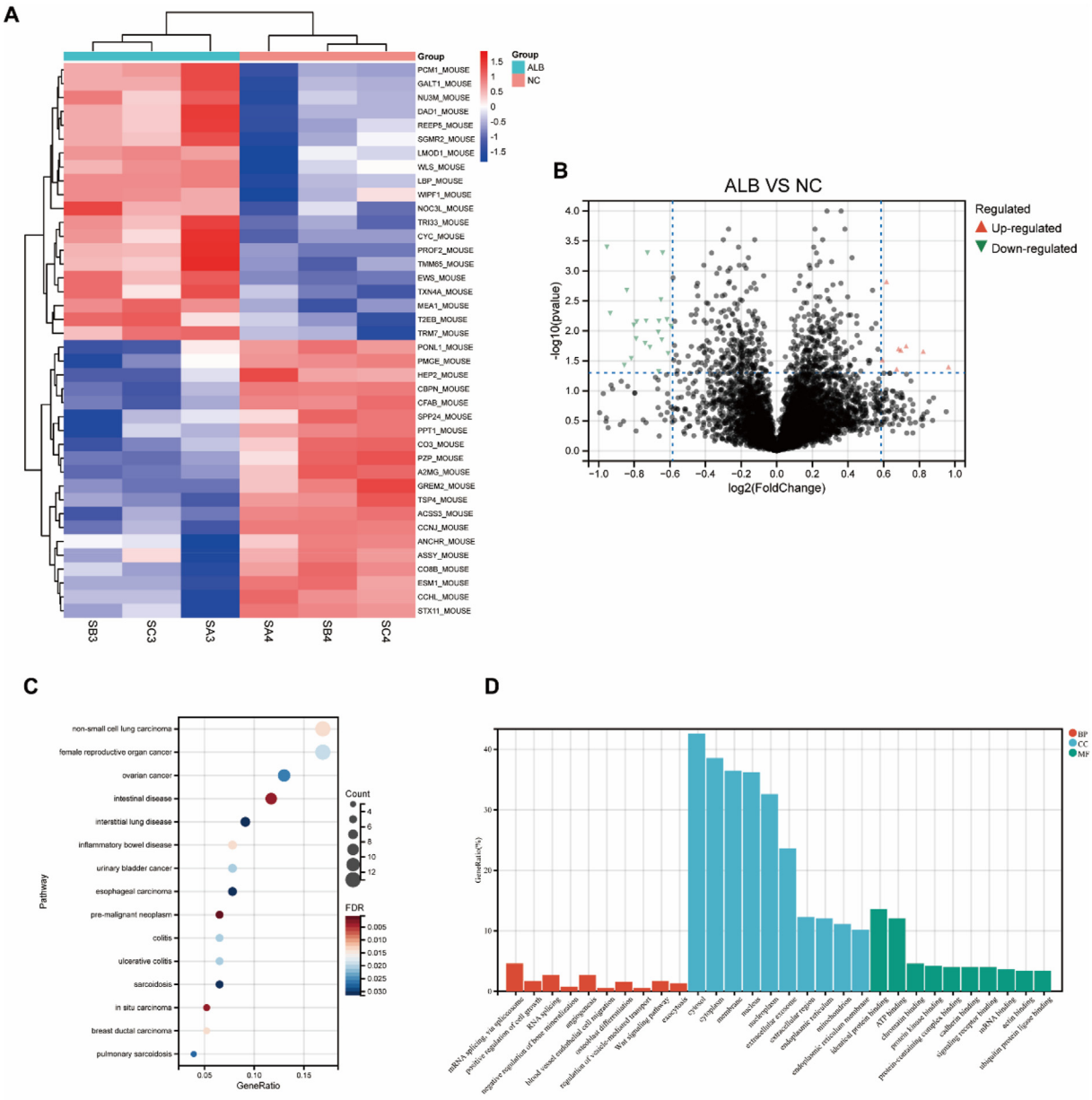

Fig. 8. (A) Heatmap and (B) Volcano plot were utilized to display the differentially expressed genes. (C–D) Pathway enrichment results of differentially expressed genes.

Exos derived miR-21-5p, thereby inducing angiogenesis and bone regeneration. Moreover, the precise role of miR-21-5p in bone and vascular regeneration also needs to be further validated through additional proteomics investigations as well.

5. Conclusions

MSCs derived from bone marrow, when stimulated by ALB enzymatic digestion, produce Exos with enhanced capability to promote bone and vascular regeneration. Sequencing analysis also revealed that ALB enzymatic digestion may strengthen its regenerative function by upregulating the expression of miR-21-5p in Exos. Furthermore, proteomics analysis identified differential gene expressions associated with bone regeneration, angiogenesis, osteoblast differentiation, vesicle-mediated transport, and the Wnt signaling pathway, suggesting multiple mechanisms contributing to the observed effects. These findings provide a new research direction for understanding the pharmacological mechanisms of TCM and aim to create possibilities for its clinical application.

Ethics statement

This animal study was approved by the Animal Experimentation Ethics Committee of Xiamen University.

Authorship contribution statement

Zuo Renjie was involved in the study design. Zuo Renjie, Liao Quan, Ding Chenchun and Guo Zhenzhen were responsible for data collection and analysis. Zuo Renjie, Liao Quan, He Junjie and Ye Ziwei assisted in data collection and manuscript revision. Zuo Renjie and Liu Guoyan wrote the manuscript and approved the final version of the manuscript. All the authors have read and approved the final manuscript.

Data availability

Data will be made available on request.

Funding

The present study was supported by grants from The National Natural Science Foundation of China (No. 81870388), the Special Project for Marine Economic Development of Xiamen City (No.17GYY001NF01).

Declaration of competing interest

We declare that we have no financial and personal relationships with other people organizations that can inappropriately influence our work, there is no professional or other personal interest of any nature or kind in any product, service and/or compary that could beconstrued as influencing the position presented in, or the review of, the manuscript entitled.

Appendix A. Supplementary data

Supplementary data to this article can be found online at https://doi.org/10.1016/j.reth.2024.11.003.

References

[1] Palaniappan P, Baalann KP. Fracture nonunion. The Pan African Medical Journal 2021;40:93.
[2] Diomede F, Marconi GD, Fonticoli L, Pizzicanella J, Merciaro I, Bramanti P, et al. Functional relationship between osteogenesis and angiogenesis in tissue regeneration. Int J Mol Sci 2020;21(9).
[3] Zhang Y, Hao Z, Wang P, Xia Y, Wu J, Xia D, et al. Exosomes from human umbilical cord mesenchymal stem cells enhance fracture healing through HIF-1α-mediated promotion of angiogenesis in a rat model of stabilized fracture. Cell Prolif 2019;52(2):e12570.
[4] Kalluri R, LeBleu VS. The biology, function, and biomedical applications of exosomes. Science (New York, NY) 2020;(6478):367.
[5] Wu D, Chang X, Tian J, Kang L, Wu Y, Liu J, et al. Bone mesenchymal stem cells stimulation by magnetic nanoparticles and a static magnetic field: release of exosomal miR-1260a improves osteogenesis and angiogenesis. J Nanobiotechnol 2021;19(1):209.
[6] Liu L, Liu Y, Feng C, Chang J, Fu R, Wu T, et al. Lithium-containing biomaterials stimulate bone marrow stromal cell-derived exosomal miR-130a secretion to promote angiogenesis. Biomaterials 2019;192:523–36.
[7] Liao W, Ning Y, Xu H-J, Zou W-Z, Hu J, Liu X-Z, et al. BMSC-derived exosomes carrying microRNA-122-5p promote proliferation of osteoblasts in osteonecrosis of the femoral head. Clin Sci (Lond) 2019;133(18):1955–75.
[8] Bitencourt TA, Hatanaka O, Pessoni AM, Freitas MS, Trentin G, Santos P, et al. Fungal extracellular vesicles are involved in intraspecies intracellular communication. mBio 2022;13(1):e0327221.
[9] Xia Y, Rao L, Yao H, Wang Z, Ning P, Chen X. Engineering macrophages for cancer immunotherapy and drug delivery. Adv Mater 2020;32(40):e2002054.
[10] Li S, Yang K, Cao W, Guo R, Liu Z, Zhang J, et al. Tanshinone IIA enhances the therapeutic efficacy of mesenchymal stem cells derived exosomes in myocardial ischemia/reperfusion injury via up-regulating miR-223-5p. J Contr Release: Official Journal of the Controlled Release Society 2023;358:13–26.
[11] Wu P, Jiao F, Huang H, Liu D, Tang W, Liang J, et al. Morinda officinalis polysaccharide enable suppression of osteoclastic differentiation by exosomes derived from rat mesenchymal stem cells. Pharmaceut Biol 2022;60(1):1303–16.
[12] Ding C, Hao M, Ma S, Zhang Y, Yang J, Ding Q, et al. Identification of peptides with antioxidant, anti-lipoxygenase, anti-xanthine oxidase and anti-tyrosinase activities from velvet antler blood. Lebensm Wiss Technol 2022;168:113889.
[13] Sun H, Xiao D, Liu W, Li X, Lin Z, Li Y, et al. Well-known polypeptides of deer antler velvet with key actives: modern pharmacological advances. N Schmied Arch Pharmacol 2024;397(1):15–31.
[14] Ho T-J, Tsai W-T, Wu J-R, Chen H-P. Biological activities of deer antler-derived peptides on human chondrocyte and bone metabolism. Pharmaceuticals 2024;17(4).
[15] Hao M, Peng X, Sun S, Ding C, Liu W. Chitosan/sodium alginate/velvet antler blood peptides hydrogel promoted wound healing by regulating PI3K/AKT/mTOR and SIRT1/NF-κB pathways. Front Pharmacol 2022;13:913408.
[16] Ma S, Ding Q, Xia G, Li A, Li J, Sun P, et al. Multifunctional biomaterial hydrogel loaded with antler blood peptide effectively promotes wound repair. Biomedicine Pharmacotherapy Biomedecine Pharmacotherapie 2024;170:116076.
[17] Wang T, Luo E, Zhou Z, Yang J, Wang J, Zhong J, et al. Lyophilized powder of velvet antler blood improves osteoporosis in OVX-induced mouse model and regulates proliferation and differentiation of primary osteoblasts via Wnt/β-catenin pathway. J Funct Foods 2023;102:105439.
[18] Tseng S-H, Sung H-C, Chen L-G, Lai Y-J, Wang K-T, Sung C-H, et al. Effects of velvet antler with blood on bone in ovariectomized rats. Molecules 2012;17(9):10574–85.
[19] Liu Y-Y, Ding Y-F, Sui H-J, Liu W, Zhang Z-Q, Li F. Pilose antler (Cervus elaphus Linnaeus) polysaccharide and polypeptide extract inhibits bone resorption in high turnover type osteoporosis by stimulating the MAKP and MMP-9 signaling pathways. J Ethnopharmacol 2023;304:116052.
[20] Greening DW, Xu R, Ji H, Tauro BJ, Simpson RJ. A protocol for exosome isolation and characterization: evaluation of ultracentrifugation, density-gradient separation, and immunoaffinity capture methods. Methods Mol Biol 2015;1295:179–209.
[21] Helwa I, Cai J, Drewry MD, Zimmerman A, Dinkins MB, Khaled ML, et al. A comparative study of serum exosome isolation using differential ultracentrifugation and three commercial reagents. PLoS One 2017;12(1):e0170628.
[22] Huang Y, Yang Y, Wang J, Yao S, Yao T, Xu Y, et al. miR-21-5p targets SKP2 to reduce osteoclastogenesis in a mouse model of osteoporosis. J Biol Chem 2021;296:100617.
[23] Ma S, Zhang A, Li X, Zhang S, Liu S, Zhao H, et al. MiR-21-5p regulates extracellular matrix degradation and angiogenesis in TMJOA by targeting Spry1. Arthritis Res Ther 2020;22(1):99.
[24] Yang S-S, Oh J-M, Chun S, Kim B-S, Kim CS, Lee J. Tauroursodeoxycholic acid induces angiogenic activity in endothelial cells and accelerates bone regeneration. Bone 2020;130:115073.
[25] Hu K, Olsen BR. Osteoblast-derived VEGF regulates osteoblast differentiation and bone formation during bone repair. J Clin Investig 2016;126(2):509–26.
[26] Ju GuiChun JG, Huang Wei HW, Liu Hui LH, Zhang AiWu ZA. Inorganic elements and nutritional components in pilose antler of Sika Deer. 2012.
[27] Li C. Deer antler renewal gives insights into mammalian epimorphic regeneration. Cell Regen 2023;12(1):26.
[28] Feleke M, Bennett S, Chen J, Hu X, Williams D, Xu J. New physiological insights into the phenomena of deer antler: a unique model for skeletal tissue regeneration. Journal of Orthopaedic Translation 2021;27:57–66.
[29] Qian Z, Zhang Y, Kang X, Li H, Zhang Y, Jin X, et al. Postnatal conditional deletion of Bmal1 in osteoblasts enhances trabecular bone formation via increased BMP2 signals. J Bone Miner Res: The Official J Am Soc Bone Mineral Res 2020;35(8):1481–93.
[30] Mishina Y, Starbuck MW, Gentile MA, Fukuda T, Kasparcova V, Seedor JG, et al. Bone morphogenetic protein type IA receptor signaling regulates postnatal osteoblast function and bone remodeling. J Biol Chem 2004;279(26):27560–6.
[31] Gargalionis AN, Adamopoulos C, Vottis CT, Papavassiliou AG, Basdra EK. Runx2 and polycystins in bone mechanotransduction: challenges for therapeutic opportunities. Int J Mol Sci 2024;25(10).
[32] Komori T. Whole aspect of Runx2 functions in skeletal development. Int J Mol Sci 2022;23(10).
[33] Makris K, Mousa C, Cavalier E. Alkaline phosphatases: biochemistry, functions, and measurement. Calcif Tissue Int 2023;112(2):233–42.
[34] Kaji H, Sugimoto T, Kanatani M, Fukase M, Kumegawa M, Chihara K. Retinoic acid induces osteoclast-like cell formation by directly acting on hemopoietic blast cells and stimulates osteopontin mRNA expression in isolated osteoclasts. Life Sci 1995;56(22):1903–13.
[35] Chen J, Singh K, Mukherjee BB, Sodek J. Developmental expression of osteopontin (OPN) mRNA in rat tissues: evidence for a role for OPN in bone formation and resorption. Matrix 1993;13(2):113–23.
[36] Rodriguez DE, Thula-Mata T, Toro EJ, Yeh Y-W, Holt C, Holliday LS, et al. Multifunctional role of osteopontin in directing intrafibrillar mineralization of collagen and activation of osteoclasts. Acta Biomater 2014;10(1):494–507.
[37] Cheng X, Yin C, Deng Y, Li Z. Exogenous adenosine activates A2A adenosine receptor to inhibit RANKL-induced osteoclastogenesis via AP-1 pathway to facilitate bone repair. Mol Biol Rep 2022;49(3):2003–14.
[38] Krylova SV, Feng D. The machinery of exosomes: biogenesis, release, and uptake. Int J Mol Sci 2023;24(2).
[39] Wu X-D, Kang L, Tian J, Wu Y, Huang Y, Liu J, et al. Exosomes derived from magnetically actuated bone mesenchymal stem cells promote tendon-bone healing through the miR-21-5p/SMAD7 pathway. Materials Today Bio 2022;15:100319.
[40] Sikora M, Śmieszek A, Pielok A, Marycz K. MiR-21-5p regulates the dynamic of mitochondria network and rejuvenates the senile phenotype of bone marrow stromal cells (BMSCs) isolated from osteoporotic SAM/P6 mice. Stem Cell Res Ther 2023;14(1):54.
[41] Guo N, Yu Y, Chu Y, Lou Q, Huang W, Wu L, et al. miR-21-5p and canonical Wnt signaling pathway promote osteoblast function through a feed-forward loop induced by fluoride. Toxicology 2022;466:153079.
[42] Liu F, Li T, Zhan X. Silencing circular RNAPTPN12 promoted the growth of keloid fibroblasts by activating Wnt signaling pathway via targeting microRNA-21-5p. Bioengineered 2022;13(2):3503–15.